Comparative study of corrosion behaviour of copper and copper–bismuth alloy in neutral aerated chloride solution

E. Ivaškevič, M. Gladkovas, A. Steponavičius, K. Leinartas and A. Sudavičius

Institute of Chemistry, Goštauto 9, 2600 Vilnius, Lithuania

The electrochemical behaviour of Cu and Cu–Bi alloys containing different amounts of Bi in aerated neutral 5% NaCl solution was investigated in the cathodic and anodic ranges and at the corrosion potential. In the cathodic range where the reduction of oxygen takes place, the experimental evidence for the suppression of this process on Cu–Bi alloys was obtained. In the anodic range, dissolution of Cu and Cu–Bi alloys occurs in a different way depending on whether these specimens have been cathodically treated before anodic sweeps or not. Corrosion currents were calculated using the anodic Tafel slope and the polarization resistance. They were found to decrease with time and to be a certain function of Bi content in alloy. XPS spectra showed that the surface layer of a corroding specimen is mainly composed of cuprous oxide, bismuth oxide and, with a high degree of probability, of elemental copper formed most likely by redeposition. Chlorine bonding to the oxygenated species of metals was presumed to be possible. In terms of the Marcus concept, Bi in the pair Cu–Bi can be attributed to a rather weak passivity promoter. Its effect on passivation enhancement is likely explained by formation of 3D oxide Bi_2O_3 involved in the composition of a passivating layer formed on the surface of a corroding alloy.

Key words: copper, copper-bismuth alloys, corrosion, surface analysis, chloride solution

1. INTRODUCTION

Owing to a wide range of technical applications of Cu in the process equipments and also in the production of various devices of electrical, electronical or magnetic purposes, extensive efforts have already been directed to investigating the electrochemically assisted corrosion of this metal. A general overview of the literature on this problem is presented in reviews [1–4].

In the past several decades, intensive studies have been carried out on the corrosion behaviour of Cu in acidic solutions. Particularly, it has been shown that corrosion of Cu in naturally aerated solutions occurs through the so-called catalytic mechanism [5]. The main stages of this mechanism were shown to be the formation of Cu(I) species, their diffusion to the bulk solution phase, and the chemical reaction with O_2 dissolved in a solution:

$$Cu \rightarrow Cu^+ + e, \quad (1)$$

$$4\ Cu(I) + 4\ H^+ + O_2 = 2\ Cu(II) + 2\ H_2O. \quad (2)$$

Only a minor part of dissolved O_2 is electrochemically reduced directly on the Cu surface:

$$O_2 + 2H_2O + 4e \rightarrow 4OH^-. \quad (3)$$

Because of reaction (2), voltammetric measurements will yield undersized values of the Cu corrosion rate [5]. In addition, the disproportionation reaction of Cu(I) and the cathodic reduction of Cu(II) to Cu(I) can also occur at the Cu surface along with reactions (1) and (2):

$$2\ Cu(I) \rightarrow Cu(II) + Cu(0), \quad (4)$$

$$Cu(II) + e \rightarrow Cu(I). \quad (5)$$

The mechanism and kinetics of Cu corrosion depend on the relations between the rates of separate reactions (1)–(5) and also on the mass transfer involving the corresponding reacting species.

Many of the published work on the corrosion behaviour of Cu are devoted to study its corrosion in chloride-containing media [6–21]. In the case of neutral solutions, according to Pourbaix diagrams in-

soluble Cu corrosion products are expected to form on Cu surface [1]. The presence of surface layers introduces additional complexity with respect to Cu corrosion in acidic chloride solutions where corrosion products are soluble [4]:

$$Cu + Cl^- \rightarrow CuCl_{ads} + e, \quad (6)$$

$$CuCl_{ads} \rightarrow CuCl_{film}. \quad (7)$$

Depending on the conditions of corrosion, Cu(I) will enter the solution either directly from the adsorbed species:

$$CuCl_{ads} + Cl^- \rightarrow CuCl^-_2, \quad (8)$$

or due to dissolution of chloride film:

$$CuCl_{film} + Cl^- \rightarrow CuCl^-_2. \quad (9)$$

The decrease of Cu corrosion rate in a naturally aerated chloride solution is believed to be due to the formation of cuprous oxide:

$$2CuCl_2^- + 2OH^- \rightarrow Cu_2O + H_2O + 4Cl^-, \quad (10)$$

which can be further oxidized to the less protective cupric hydroxychloride:

$$Cu_2O + \tfrac{1}{2}O_2 + Cl^- + 2H_2O \rightarrow Cu_2(OH)_3Cl + OH^-. \quad (11)$$

The overall corrosion process is controlled by mass transfer involving such species as O_2, Cl^-, OH^-, Cu^+ and $CuCl_2^-$ to and from the Cu corroding surface.

In the fields of Cu corrosion protection and of the improvement of other Cu properties, the effect of alloying elements (AEs) being observed, in some instances, even at low contents, has been studied rather extensively from the fundamental and technical points of view [2, 3, 21–24]. As in the case of pure Cu, the Cl–containing solutions have often been used as the corrosive media as well [9, 10, 17, 24–27].

In regard to the alloying elements, due attention should by given to the considerations by Marcus [28] on some factors in the effect of AEs on the passivation of alloys. These factors were proposed to include the metal–oxygen bond strength, $\varepsilon_{M\text{-}O}$, and the metal–metal bond strength, $\varepsilon_{M\text{-}M}$. In particular, it has been suggested that AEs can play at least a double role depending on the balance between $\varepsilon_{M\text{-}M}$ and the heat of adsorption of oxygen: (*i*) of passivity promoters, which can be defined as AEs possessing a high heat of adsorption of oxygen together with a relatively low $\varepsilon_{M\text{-}M}$, because transition from the adsorbed overlayer to 3D oxide requires an easy disruption of M–M bond; (*ii*) of dissolution moderators, which can be defined as AEs possessing higher values of $\varepsilon_{M\text{-}M}$, because this increases the activation energy barrier for dissolution.

Cu forms a number of different alloys, several of them being of great technological importance. Although Cu–Bi alloys (Bi and Cu form a system with a simple eutectic and no intermediate phases) do not belong to the alloys of considerable current use [21–24], several observations presented in the literature are worth noting. It was recognized that, for example, Cu–Mn–Bi alloy exhibits a rather strong ferromagnetism [29]. Bi was proposed to be used to increase the resistance of Cu to corrosion [30]. However, it was also pointed out that the latter finding is largely empirical. Therefore, a more systematic investigation of the effect of Bi on the corrosion behaviour of Cu seems to be of a justified interest.

Lack of available data on the effect of Bi on the corrosion behaviour of Cu layer stimulated the present work. In this paper, we report the results of a preliminary investigation of the corrosion behaviour of freshly electrodeposited Cu–Bi alloys in a naturally aerated neutral 5% NaCl solution by the electrochemical and X-ray photoelectron spectroscopy (XPS) techniques.

2. EXPERIMENTAL

2.1. Materials and solutions

Solutions destined for deposition of Cu or Cu–Bi layers were prepared from doubly distilled water, highest purity H_2SO_4 and analytical grade $CuSO_4 \cdot 5H_2O$; the latter reagent was additionally purified by heating at 300 °C for 3 h.

0.5 M H_2SO_4 + 0.5 M $CuSO_4$ and 0.5 M H_2SO_4 + + 0.1 M $CuSO_4$ solutions were used in our experiments. The first solution was applied to obtain a copper underlayer (10 mA cm^{-2}, t = 5 min) onto a polycrystalline smooth Pt electrode and the second one to obtain a Cu layer applied for a comparison and after addition of an appropriate amount of Bi^{3+} – to deposit a Cu–Bi layer (5 mA cm^{-2}, various t) which was deposited onto a Cu-covered Pt electrode. In the latter case, the working solution was obtained by addition of an appropriate volume of a stock 0.1 M Bi^{3+} solution prepared by dissolution of analytical grade $Bi(NO_3)_3 \cdot 3H_2O$ in highest purity HNO_3 (1:1). Both sulphate solutions were deoxygenated with high purity argon.

The corrosion medium was a naturally aerated neutral 5% NaCl solution prepared from analytical grade salt and doubly distilled water.

2.2. Electrochemical measurements

a) *Cell and electrodes*. The electrochemical measurements were performed at 298 K in a thermostatically controlled water-jacketed three-electrode corrosion cell. The working electrode was a vertical polycrystalline Pt disc (the area of exposed surface 1.0 cm^2). A platinum electrode (≈4 cm^2) and an Ag/AgCl/KCl(sat.) electrode were used as the counter and the reference electrodes, respectively. The reference electrode was placed in a separate cell and connected to the corrosion cell through a salt bridge with a Luggin capillary tip in the corrosion cell. All potentials (E) are quoted here related to the standard hydrogen electrode (SHE).

Two series of experiments were performed in our work. In the first series, the Pt electrode covered with a Cu underlayer, (Pt)Cu_o, was coated with a Cu–Bi alloy layer, (Pt)Cu–Bi, and afterwards was applied for the corrosion test. In the second series conducted for comparison, the (Pt)Cu_o electrode was coated additionally with a Cu layer, (Pt)Cu.

b) *Apparatus.* The measurements were carried out using a computerized PS-305 potentiostat (Elchema). The polarization curves and the corrosion parameters were computed after each experiment using a VOLTSCAN program.

c) *Calculation of corrosion parameters.* Corrosion behaviour of Cu and Cu–Bi alloys was evaluated by estimating the polarization resistance (R_p) [31]. In some instances, the instantaneous corrosion current (I_{cor}) was also calculated.

As is commonly accepted, the polarization resistance R_p is defined as

$$R_p = (\mathrm{d}I/\mathrm{d}\Delta E)^{-1}_{\Delta E=0}. \quad (12)$$

R_p was calculated here from the polarization curves recorded by a single triangular potential sweep within the range $E_{cor} \pm 5$ mV at a scan rate of 0.1 mV s^{-1} (the potential scan was initiated in the negative direction).

I_{cor} can be evaluated using a simplified equation [32]:

$$I_{cor} = b_a/2.3R_p, \quad (13)$$

where b_a is the anodic Tafel slope. The anodic Tafel slope b_a was evaluated from the potentiostatic transients in freely aerated 5% NaCl solution, taking practically steady values of the current, which were further used to prepare a semilogarithmic $\Delta E/\log i$ plot.

Since the conductivity of 5% NaCl solution is high, no correction for the uncompensated solution resistance, R_u, was applied.

2.3. Surface analysis

An *ex situ* X-ray photoelectron spectroscopy (XPS) analysis was carried out for the following specimens: (*i*) freshly deposited Cu; (*ii*) a freshly deposited Cu–Bi alloy layer; (*iii*) the specimens as in (*i*) or (*ii*) after immersion for different time in the 5% NaCl solution. The test layers 0.2–0.5 μm thick were deposited galvanostatically as described above onto mechanically polished Cu plates (1 x 1 cm). After preparation, the specimens were immediately stored in the analysis chamber, the exposure time to room atmosphere being less than 2 min.

To examine elemental surface stoichiometries, the Cu $2p_{3/2}$, O *1s*, Cl $2p_{3/2}$, and Bi $4f_{7/2}$ XPS spectra were recorded on a VG ESCALAB MK II spectrometer (MgK_α 1253.6 eV, pass energy of 20 eV) interfaced to an IBM PC/XT for data acquisition. The electron take off was at 90 ° to the specimen surface, giving a typical depth of analysis of no less than 1 nm. The binding energy (E_b) values were calibrated with respect to the C *1s* signal at 284.6 eV. The binding energies of the Cu $2p_{3/2}$ electrons were taken as 932.4 ± 0.2 eV in metallic Cu, as 932.3 ± 0.2 eV in Cu_2O and as 933.0 ÷ 933.8 eV in CuO [33], and the kinetic energies of the Cu $L_3M_{45}M_{45}$ Auger electrons in copper metal as 919.0 eV, in Cu_2O as 917.2 ÷ 916.2 eV and in CuO as 917.9 ÷ 918.1 eV [33, 34]. E_b of the Bi $4f_{7/2}$ electrons of bismuth metal was taken as 156.8 ± 0.2 eV [33, 34] and that for Bi compounds as follows: in Bi_2O_3 as 158.5 eV [33], in BiOCl as 159.6 eV [33], and in $Bi_2O_4 \cdot 2H_2O$ as 159.0 eV [33]. Elemental surface stoichiometries were obtained from a peak area ratios corrected by sensitivity factors reported in [34]. Estimating the composition of the surface films, it was also assumed that the effective escape depths for each element were sufficiently close to one another.

The depth distribution of elements was examined from the XPS measurements after an Ar^+ ions sputtering (ultra-high pure Ar^+ ions beam, an accelerating voltage of 1 kV). The etching current was maintained at the level of *ca*. 20 μA cm^{-2} or ~4 nm min^{-1}. The sputtering depth was proportional to the sputtering time (t_s).

Each reported value is the average of at least three determinations.

3. RESULTS AND DISCUSSION

3.1. Open-circuit potentials

Open-circuit potentials ($E_{i=0}$) in the unstirred aerated 5% NaCl solution for freshly deposited pure Cu and Cu–Bi (ca.0.4 at%) specimens are presented as a function of immersion time (t_{imm}) in Fig. 1. One

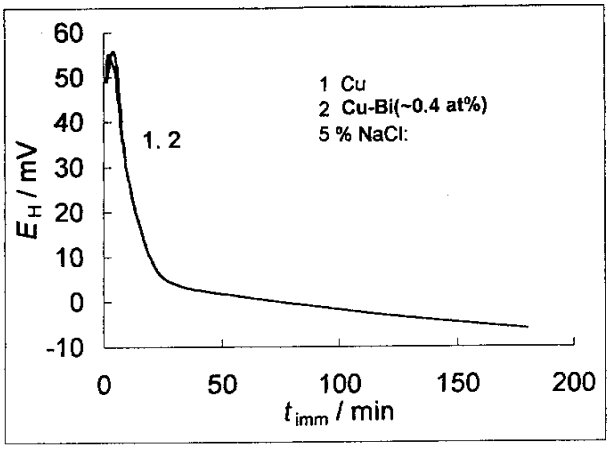

Fig. 1. Variation of corrosion potential (open-circuit potential) of copper and copper–bismuth alloy with immersion time in neutral aerated 5% NaCl solution

can see that the Cu–Bi alloy electrode behaved quite similarly to the Cu electrode. In either case, the potential initially shifted in the cathodic direction with increasing t_{imm}, in agreement with the earlier observations related to the Cu samples, behaviour in the chloride medium for a shorter t_{imm} [6, 19, 35]. For a longer t_{imm}, this potential change slowed down and $E_{i=0}$ became almost constant after a lapse of time of about 25 min. Therefore, when the Cu and Cu–Bi alloy electrodes were allowed to corrode freely in 5% NaCl solution, the corrosion behaviour was almost the same, that is, under our experimental conditions, virtually no Bi effect on the Cu corrosion was established.

3.2. Voltammetric investigation

The O_2 reduction limiting current density under the steady-state conditions was evaluated from the relationship

$$i_{lim} = -nFcD/\delta. \quad (14)$$

Taking the diffusion coefficient, D, for O_2 as $2 \cdot 10^{-5}$ cm^2 s^{-1} [6], the concentration, c, of dissolved O_2 as $1.75 \cdot 10^{-7}$ mol cm^{-3} [2] (at a partial pressure of O_2 of 0.2 bar in the earth's atmosphere provided the system conformed to the Henry's law and also having regard to a solubility of oxygen in the chloride solution used here), $n = 4$ and the thickness of diffusion layer, δ, as $5 \cdot 10^{-2}$ cm, it was obtained that $i_{lim,calc} \approx 0.027$ mA cm^{-2}. In accordance with considerations reported in [6], a similar behaviour of bare and Cu_2O-covered Cu with respect to O_2 reduction was assumed.

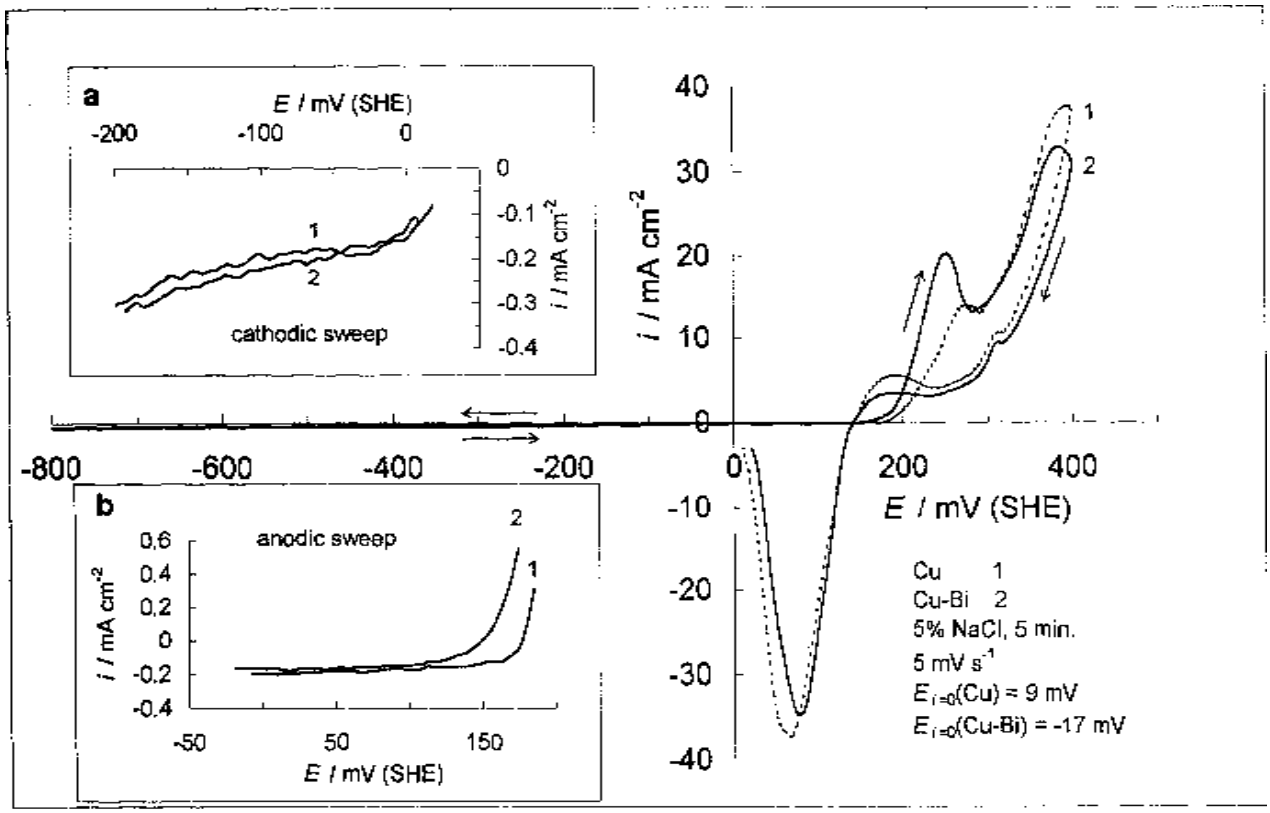

Fig. 2. Cyclic linear sweep voltammograms for Cu and Cu–Bi (*ca*. 0.7 at.%) alloy electrodes in aerated 5% NaCl solution. The 1st scan curves recorded after 5 min immersion in the same solution starting from open-circuit potential in the cathodic direction. Parts of cyclic curves in enlarged scale are shown in the insets *a* (cathodic sweep) and *b* (anodic sweep)

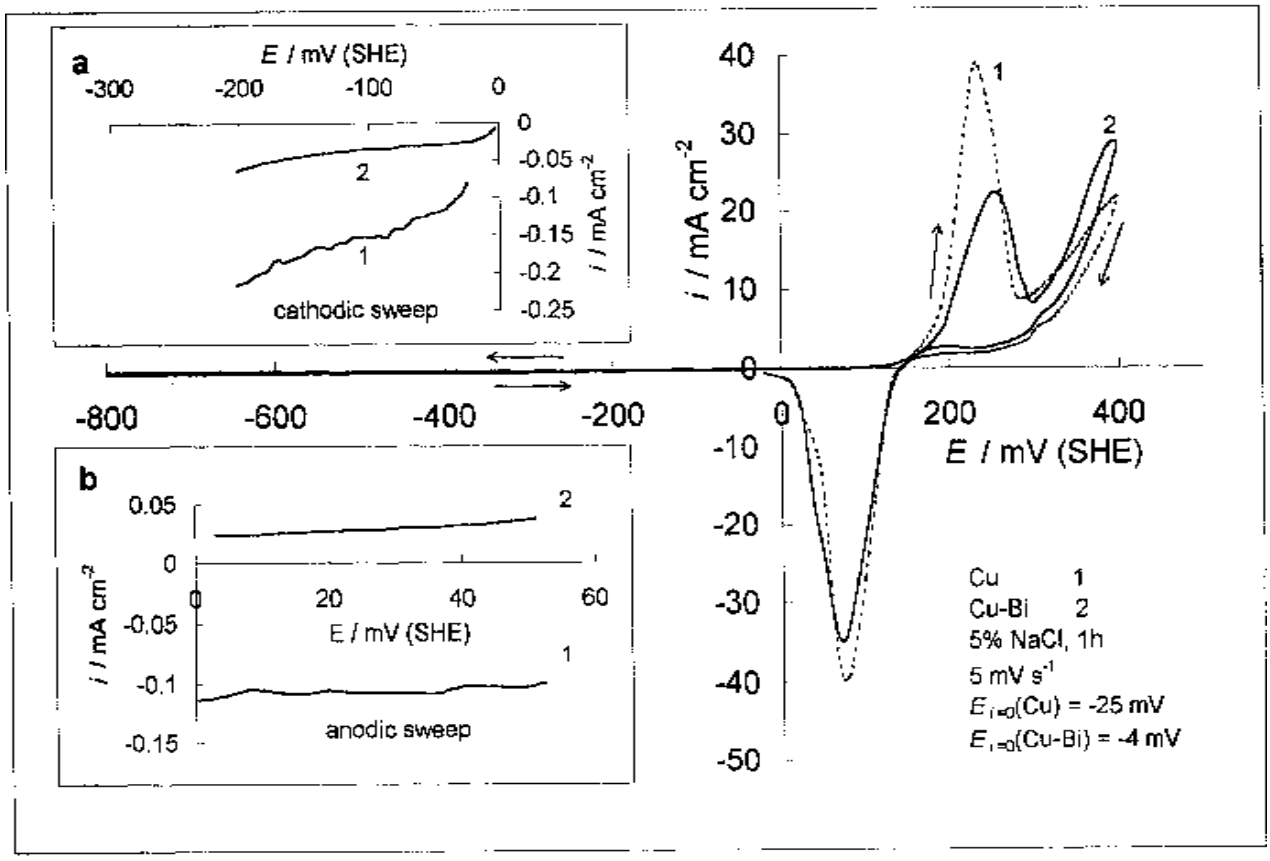

Fig. 3. The same as in Fig. 2, but curves recorded after 1 h immersion

The cyclic *i*/*E* curves for Cu and Cu–Bi(*ca*.0.7 at%) in 5% NaCl solution were recorded after various immersion times (5 min and 1 h at open-circuit) by a singular triangular potential sweep starting from $E_{i=0}$ in the negative direction between the cathodic switching potential of –0.80 V and the anodic one of +0.40 V (Figs. 2, 3). In a relatively good agreement with the data reported by Deslouis et al. [6], the shape of polarization curves for a Cu electrode depends on the t_{imm} in chloride solution. In particular, the potential scan in the negative direction from $E_{i=0}$ up to E = –200 mV presents the initial branch of the curve with a rather steadily increasing current (insets *a* to Figs. 2 and 3) that corresponds most likely to the O_2 reduction process. Comparison of the currents in this range of ΔE shows that the current is higher for the shorter t_{imm} (inset *a* to Fig. 2) than for the longer t_{imm} (the inset *a* to Fig. 3).

Considering the initial cathodic *i*/*E* profile for the Cu–Bi electrode, it can be seen that this electrode behaves similarly relative to t_{imm}, as the Cu electrode (insets *a* to Figs. 2, 3, curves *2*). In addition, it was also found that, in the event of the longer t_{imm}, the cathodic current density within the *E* range under discussion was significantly lower than that at the Cu electrode (inset *a* to Fig. 3).

In order to obtain more versatile information on the anodic dissolution of Cu and Cu–Bi alloy, the anodic polarization curves for the specimens that underwent high potentiodynamic cathodic polarization (Figs. 2, 3) were compared with the curves recorded for cathodically untreated specimens (Figs. 4, 5). It was supposed that if the potential was anodically scanned from –0.80 V to $E_{i=0}$, the surface of

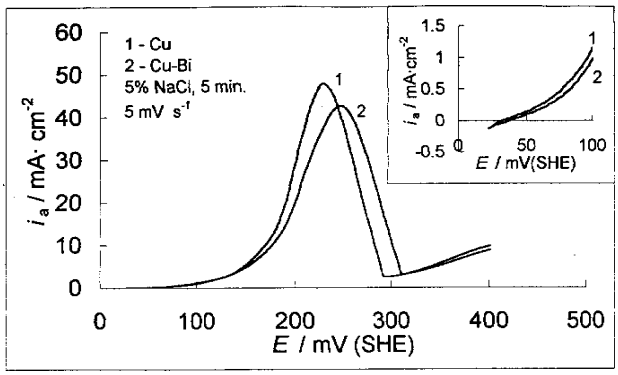

Fig. 4. Anodic current–potential curves for Cu and Cu–Bi (*ca*. 0.7 at.%) alloy electrodes in aerated 5% NaCl solution. Curves recorded after 5 min immersion in the same solution. Inset shows initial parts of curves in enlarged scale

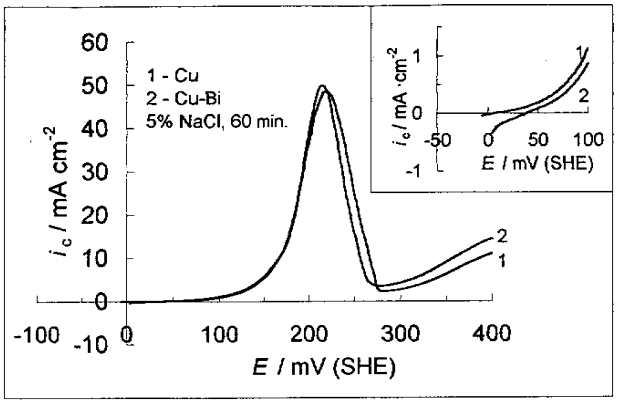

Fig. 5. The same as in Fig. 4, but curves recorded after 1 h immersion

both specimens would become cleaner than in the case of the anodic scan starting from $E_{i=0}$.

The experimental data obtained here with the cathodically treated electrodes (Figs. 2, 3) show that the *i*/*E* profiles at potentials positive of the $E_{i=0}$ have some features that are worth mentioning.

Firstly, in the *E* region bounded by the $E_{i=0}$ estimated initially and that value of *E* at which an abrupt increase in the anodic current is observed, the run of the *i*/*E* curve depends on t_{imm}. While at t_{imm} = 5 min these initial branches of polarization curves are quite similar and the low cathodic current densities are detected for both electrodes (inset *b* to Fig. 2), the analogous *i*/*E* profiles are different for the longer t_{imm} (inset *b* to Fig. 3). In the latter case, the cathodic current is also observed for the Cu specimen, as in the previous case. However, for the Cu–Bi electrode, the low (of an order of several hundredth of mA cm^{-2}) anodic current was registered over the whole *E* range of interest (curve *2*) indicating a weak oxidation process that under other conditions had been not observed.

Furthermore, the further positive scan, in particular from *ca*. +0.10 V to +0.40 V, results in the appearance of two anodic current peaks at +0.22... +0.25 V and E > +0.35 V (the latter peak is imperfectly plotted here). Mention may be made of the observations reported by de Chialvo et al. [36]. They observed three anodic current peaks in the *E* range close to that we analyzed here. Most likely one of the reasons for such a difference is that the cited authors registered the stabilized *i*/*E* profile in a solution with pH 9. It should be also pointed out that the upper limit of the positive *E* scan applied in our work is significantly lower than the critical value of *E* corresponding to an abrupt increase in the anodic current due to a passivating film breakdown [36].

Finally, it was found that the position and the height of these anodic current peaks depended on the nature of the specimens and on t_{imm} (Figs. 2, 3). Whereas the first current peak for the Cu electrode increased from 14 mA cm^{-2} for t_{imm} = 5 min to 38 mA cm^{-2} for t_{imm} = 1 h, the height of the current peak registered at the Cu–Bi electrode remained almost unchanged. The peak potential $E_{pa,1}$ for the pure Cu electrode shifted toward more negative values by about 40 mV with this prolongation of the length of immersion. The analogous analysis for the second wave (made here for the current density at E = +0.40 V) showed that *i* for the Cu electrode is higher by *ca*. 16% than that for the Cu–Bi electrode, when the both electrodes were treated potentiodynamically after a short-time corrosion process (Fig. 2). The prolongation of t_{imm} reduced the current density by a factor of *ca*. 1.8 at the Cu electrode, but only slightly reduced *i* at the Cu–Bi electrode. Consequently, the anodic dissolution of the electrodes applied in our work was found to be sensitive both to the presence of alloying element and to the length of the preceding exposure of metals to a corrosive medium. The effect of the latter factor should be particularly emphasized.

Voltammetric measurements were also performed to enlighten the role of the corrosion products film which formed on the surface of Cu and Cu–Bi alloy in the 5% NaCl solution and which did not undergo cathodic reduction. As is clear from a comparison of the data presented in Figs. 2, 3 and Figs. 4, 5, the anodic behaviour of the specimens untreated cathodically is quite different from that after cathodic polarization. Within the same region of anodic polarization, a single well-defined current peak was revealed (Figs. 4, 5) instead of two peaks observed after cathodic polarization (Figs. 2, 3). Besides, the *i*/*E* profiles for the both specimens are rather similar regardless of the change in t_{imm}. Somewhat slightly different potentiodynamic responses for the Cu and Cu–Bi electrodes were recorded only in the case of short-time immersion (Fig. 4). The peak potentials in Figs. 4, 5 are close to the $E_{pa,1}$ (Figs. 2, 3) indicating that in either case the oxidation process causing the appearance of the current peaks under consideration may be the same. At this stage, it is not clear why the second oxidation reaction occurring at a more positive *E* (Figs. 2, 3) became suppressed when cathodic polarization was not applied (Figs. 4, 5).

3.3. Corrosion parameters

The experimental values of the anodic Tafel slope b_a and of the polarization resistance R_p as functions of t_{imm} for Cu and Cu–Bi alloys are shown in Fig. 6. The results obtained show that an average value of

b_a is close to 60 mV decade^{-1} irrespective of electrode material and of t_{imm} (Fig 6*a*). Such an anodic Tafel slope can be attributed to a one-electron transfer reaction with diffusion of a reactant or product in the aqueous phase being the rate-determining step, as suggested by Kato and Pickering [37] (in our case, reaction (1)). The average value of b_a of 60 mV decade^{-1} was further used, if required.

For both Cu and Cu–Bi alloy samples in 5% NaCl solution, there is a general trend towards increasing R_p with t_{imm} (Fig. 6*b*). This behaviour is reasonable to expect in the light of the mechanism of Cu corrosion in a chloride solution that has been generally accepted at the present time [4]. The t_{imm}–dependence of R_p was found to be similar for all the specimens (Fig. 6*b*).

I_{cor} for Cu and Cu–Bi alloy samples were plotted as a function of t_{imm} (Fig. 7) and were found to agree with the time law in the form:

$$I_{cor} = kt^n_{imm}, \quad (15)$$

where k is the arbitrary instantaneous corrosion current after the specific t_{imm} taken here as 1 min. Fitted values of k and n are presented in Fig. 7. The values of n were obtained to be close to –0.5. This result is usually explained by a diffusion-controlled mass transport through a surface layer [2]. In principle, the lower values of n may be indicative of a faster decrease in the corrosion rate. Therefore, it may be expected that the value of I_{cor} as a function of t_{imm} for Cu–Bi alloys decreases somewhat faster as compared to pure Cu. Apparently the corrosion products formed on Cu–Bi alloys are more protective than in the case of pure Cu. In this connection, it can be pointed out that some other Cu alloys show a similar behaviour. For example, Cu–Ni alloys in seawater corrode at higher rates before the formation of a protective oxide film [9].

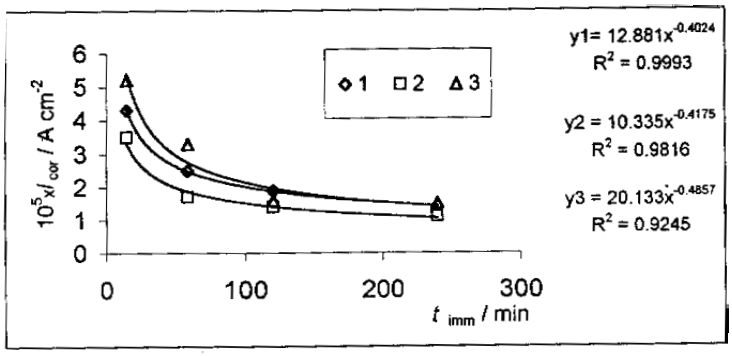

Fig. 7. Variation of instantaneous corrosion current I_{cor} with immersion time in aerated 5% NaCl solution for Cu (*1*) and Cu–Bi alloys containing *ca*. 0.4 (*2*) or ca. 0.7 at.% Bi (*3*)

On the other hand, the higher values of k can indicate that a specimen corrodes faster. Then, a comparison of the k values for Cu–Bi alloys with that for pure Cu indicates that this parameter depends on the chemical composition of alloy (Fig. 7). While no significant difference of k for Cu and Cu–Bi alloy containing the lesser content of Bi was detected, the higher content of this element caused the parameter k to increase by about 50% relative to pure Cu.

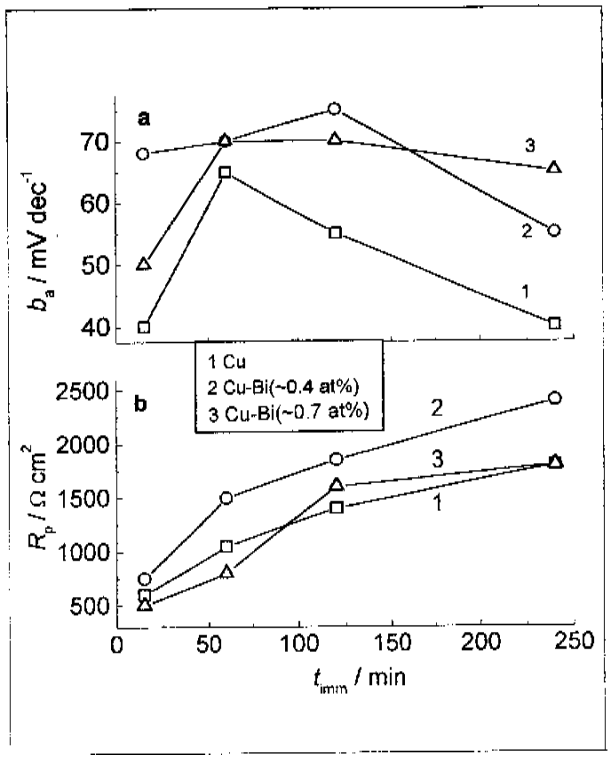

Fig. 6. Variation of anodic Tafel slope b_a (*a*) and polarization resistance R_p (*b*) with immersion time in aerated 5% NaCl solution for Cu (*1*) and Cu–Bi alloys (*2*, *3*) electrodes

3.4. Surface analysis

Electron spectroscopy, XPS and Auger experiments, are commonly used to gain information about the composition of corrosion layers and passive films on metals. Quite apparently it is most desirable to transfer a sample from the electrochemical environment to vacuum for analysis without exposure to the atmosphere. Under conditions of our experiments, the contact of Cu or Cu–Bi alloys with the atmosphere was not eliminated. Therefore, this situation was taken into account while interpreting the spectra.

The results of XPS and Auger spectroscopy measurements on a system Cu-copper oxides are in detail presented in the literature (see, *e.g.*, the pa-

pers [38–43] and the reviews [44–46]). Auger spectroscopy has been applied to study the surface composition of Cu–Bi alloys deposited from a slightly acidic EDTA solution [47].

The results of XPS analysis are summarized in Table 1. The typical photoelectron spectra from Cu and Cu–Bi alloy specimens for the individual elements are displayed in Figs. 8–11. In addition to the XPS data, Cu Auger spectra are also presented (Fig. 12).

The quantitative determination of separate elements showed that, as one would expect, the XPS spectra of the specimens untreated in the corrosive medium consisted of peaks corresponding to copper, bismuth and oxygen (Table 1). The content of Bi in the specimens increased with increasing the bulk concentration of Bi^{3+} in the sulphate solution used for electrodeposition of alloy, *viz*. it was equal to about 0.009, 0.4 and 0.7 at.% when the bulk c of Bi^{3+} was $1{\cdot}10^{-4}$, $5{\cdot}10^{-4}$ and $1{\cdot}10^{-3}$ M, respectively. It

Table 1. **Composition of surface layers of copper–bismuth alloys derived from XPS measurements**

Treatment in 5% NaCl solution	Signal from element's core level	Contents, at%		
		before etching	after 30 s etching	after 150 s etching
Sample (a): Copper–bismuth alloy (*ca*. $9.0{\cdot}10^{-3}$ at%)				
without	Cu $2p_{3/2}$	43.7	*ca*. 99.7	
	Bi $4f_{7/2}$	~$9{\cdot}10^{-3}$	very small	
	O *1s*	56.3	0.3	
t_{imm} = 30 min	Cu $2p_{3/2}$	63.3	92.5	
	Bi $4f_{7/2}$	*ca*. 0.004	*ca*. 0.07	
	O *1s*	30.2	6.6	
	Cl 2p	6.5	0.8	
t_{imm} = 60 min	Cu $2p_{3/2}$	53.3	80.4	90.6
	Bi $4f_{7/2}$	0	*ca*. 0.03	*ca*. 0.02
	O *1s*	35.2	18.6	9.2
	Cl *2p*	6.6	0.9	*ca*. 0.2
	Na 1s	5.0	0	0
Sample (b): Copper–bismuth alloy (*ca*. 0.4 at%)				
without	Cu $2p_{3/2}$	35.5	93.3	
	Bi $4f_{7/2}$	~0.4	0.1	
	O *1s*	64.1	6.6	
t_{imm} = 30 min	Cu $2p_{3/2}$	63.8	91.5	
	Bi $4f_{7/2}$	~0.1	*ca*. 0.06	
	O *1s*	24.6	7.2	
	Cl *2p*	11.4	1.3	
t_{imm} = 60 min	Cu $2p_{3/2}$	51.7	80.0	92.9
	Bi $4f_{7/2}$	*ca*. 0.06	*ca*. 0.09	*ca*. 0.02
	O *1s*	39.0	18.8	6.6
	Cl *2p*	5.5	1.1	~0.6
	Na *1s*	3.8	0	0
Sample (c): Copper–bismuth alloy (*ca*. 0.7 at%)				
without	Cu $2p_{3/2}$	51.5	95.9	
	Bi $4f_{7/2}$	~0.7	~0.2	
	O *1s*	47.8	*ca*. 3.9	
t_{imm} = 30 min	Cu $2p_{3/2}$	47.1	93.4	
	Bi $4f_{7/2}$	0.7	0.09	
	O *1s*	40.7	5.6	
	Cl *2p*	11.5	1.0	
t_{imm} = 60 min	Cu $2p_{3/2}$	53.7	76.8	85.2
	Bi $4f_{7/2}$	*ca*. 0.06	*ca*. 0.04	*ca*. 0.09
	O *1s*	35.9	20.0	14.3
	Cl *2p*	6.5	~1.9	0.5
	Na *1s*	~3.8	1.2	0

Note: Surface contents of individual elements (at%), as a rule, are given as rounded numbers.

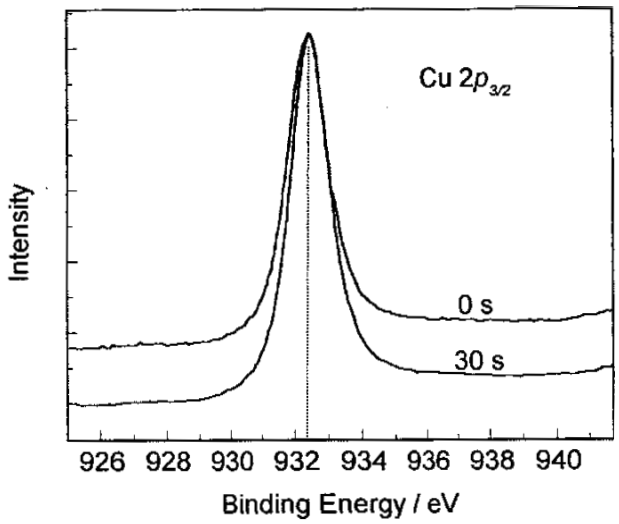

Fig. 8. X-ray photoelectron spectra (XPS) of Cu $2p_{3/2}$ from Cu–Bi (*ca*. 0.4 at.%) alloy specimen after 30 min immersion in aerated 5% NaCl solution. Numbers at signals denote the Ar ion sputtering time

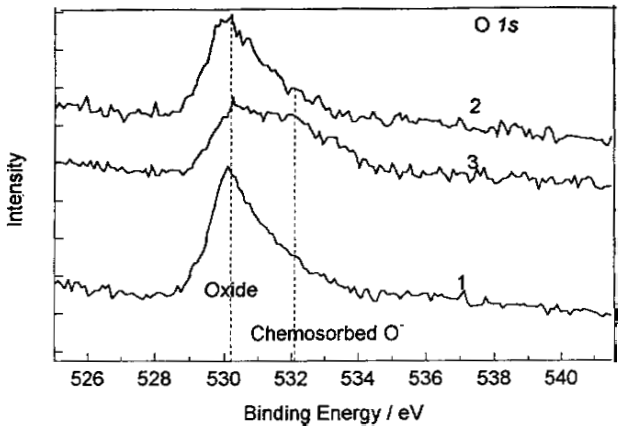

Fig. 9. XPS of O *1s* from Cu–Bi alloys specimens containing *ca*. 0.009 (*1*), ca. 0.4 (*2*) or *ca*. 0.7 (*3*) at.% Bi after 30 min immersion in aerated 5% NaCl solution

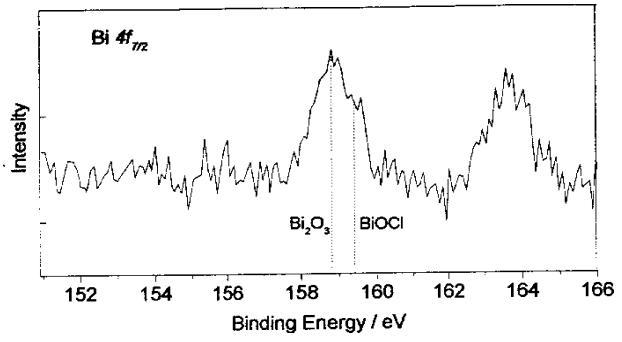

Fig. 10. XPS of Bi $4f_{7/2}$ from Cu–Bi (*ca*. 0.4 at.%) alloy specimen after 30 min immersion in aerated 5% NaCl solution.

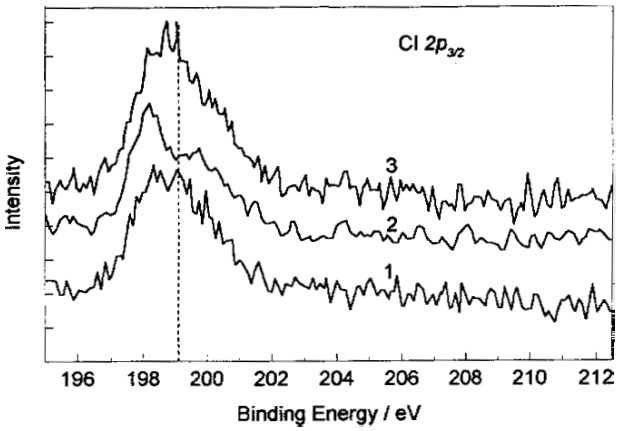

Fig. 11. XPS of Cl $2p_{3/2}$ from Cu–Bi alloys specimens containing *ca*. 0.009 (*1*), *ca*. 0.4 (*2*) or *ca*. 0.7 (*3*) at.% Bi after 30 min immersion in aerated 5% NaCl solution

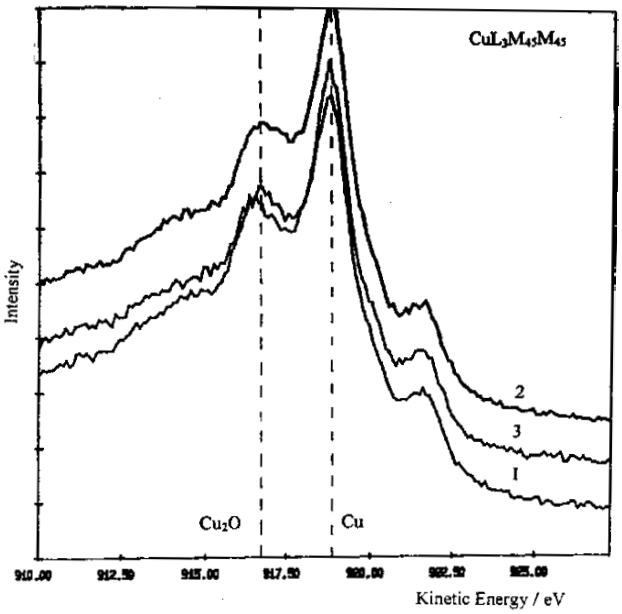

Fig. 12. Auger spectra of $CuL_3M_{45}M_{45}$ from Cu–Bi alloys after 30 min immersion in aerated 5% NaCl solution. Cu–Bi alloys with $9 \cdot 10^{-3}$ (*1*), *ca*. 0.4 (*2*) and *ca*. 0.7 at.% (*3*)

is noticeable that these quantities were found to be nearly proportional. In all cases significant amounts of oxygen were found. Because of lack of a sufficient body of data there was no possibility to establish relationships between the contents of separate elements. However, it can be easily shown that, in the case of the specimens whose corrosion behaviour was studied (see above), the oxygen content decreased as that of Bi increased (Table 1).

Figures 8, 9 and 12 show, respectively, the Cu $2p_{3/2}$ and O *1s* X-ray photoelectron spectra and Cu $L_3M_{45}M_{45}$ Auger spectra from the Cu–Bi alloy (0.4 at. %) specimen after its exposure to the aerated

5% NaCl solution for t_{imm} = 30 min. A sole peak at E_b = 932.2 eV was detected in the Cu $2p_{3/2}$ core level energy range (Fig. 8). Weak satellite peaks can be also resolved on the side of higher binding energies. The general shape of the Cu $2p_{3/2}$ XPS spectrum recorded in our work is similar to that presented by other authors [14, 41, 42].

As is customary, the data on the Cu $2p_{3/2}$ core level and the Auger spectra Cu $L_3M_{45}M_{45}$ and on the O *1s* level together with the characterization of the Cu $2p_{3/2}$ spectrum shape were used to distinguish between metallic Cu and oxidized copper, as well as between cuprous and cupric species. However, the experimental value of E_b (932.2 eV) did not allow a clear distinction between metallic Cu and Cu_2O, since it lies in essence in the ranges of E_b for the Cu $2p_{3/2}$ signals which can be considered as the respective reference values, namely, in the metal state (932.2 to 933.1 eV [33, 34, 39, 41, 42, 48–51]) and in Cu_2O (932.2 to 932.6 eV [39, 41, 42, 48]). On the other hand, this experimental E_b somewhat differs from the reference values on the Cu $2p_{3/2}$ signal in CuO (933.0 to 933.6 eV [39, 41, 45, 48]). Besides, the core level XPS spectra of the Cu *2p* line in pure Cu were observed to have only a very small asymmetry [52]. Consequently, only very small amounts of cupric species may be indicated by the presence of the weak satellites mentioned above.

Since from the same compounds, in particular from metallic Cu and Cu_2O, there is a rather significant variation in the E_b values for the main peak on the Cu $2p_{3/2}$ spectrum, difficulties emerge in choosing an arbitrary reference value of the respective E_b. In our study, the experimental value of E_b = = 932.2 eV for the Cu $2p_{3/2}$ electrons (Fig. 8) may be compared to the values of E_b in metallic Cu, 932.4 eV [33], and in Cu_2O, 932.3 eV [33] (the same Ref. was also used in [14]).

The peak width, FWHM, for the Cu $2p_{3/2}$ signal (Fig. 8) was found to vary within the ranges 1.345 to 1.404 eV at t_{imm} = 30 min and 1.367 to 1.437 eV at t_{imm} = 60 min. This XPS parameter for the Cu $2p_{3/2}$ signal is closer to that for metallic Cu (1.4 eV [39]) in comparison with Cu_2O (1.8 or 4.5 eV, depending on the kind of this reagent [39]).

To characterize additionally the surface of a specimen under study, the Cu $L_3M_{45}M_{45}$ Auger spectrum (Fig. 12) was also analyzed. Two maxima at E_k of *ca*. 918.9 and 916.7 eV were resolved on this spectrum. This suggests that the very top layers of the surface of specimen contains both Cu(0) and Cu(I), the latter being in the form of Cu_2O. In addition, in a good agreement with [39], a distinct peak at 921.6 eV was found in the Auger spectra. Due to the very short escape depths of Auger electrons, the information obtained by Auger electron spectroscopy pertains to the thinner surface layer than in the case of XPS. This factor and also the sensitivity of the Auger process to surface roughness should be taken into account when a comparison of chemical shifts in XPS and AES are made, in particular to distinguish the E_b for copper and copper oxides [44, 53].

The O *1s* photoelectron spectra (Fig. 9) are broad and asymmetric, indicating the presence of more than one type of oxygen in the surface layer. In accordance with the opinion of other authors (see, *e.g*., [38, 39]), the lower binding energy oxygen is probably attributed to oxygen in the oxide lattice, while the higher binding energy oxygen is due to another oxygen-containing species. A distinct peak at 530.2 eV can be ascribed to lattice oxygen in Cu_2O (O *1s* core binding energy of 530.4 eV [38, 48]). FWHM varied significantly at t_{imm} = 30 min (1.766 to 3.03 eV), but became almost constant at t_{imm} = 60 min (1.30 to 1.385 eV). Such a variation in FWHM of O *1s* signal can be attributed to a different structure of Cu_2O formed on the surface of corroding sample, in accordance with the observation in [39].

It may be added that the values of band gap energies for Bi_2O_3 and Cu_2O, as the quantities equivalent to, in accordance with [54], the heats of formation of these oxides, were shown to be sensitive to the formation process, the microstructure and also to the thickness of films [55].

The ill-resolved signal at *ca*. 532.1 eV suggests the presence of only small amounts of strongly chemisorbed oxygen (the reference E_b = 532.2 eV [38]).

In brief, our XPS and AES experiments indicate that the surface layer of Cu–Bi alloy specimen after exposure to aerated neutral 5% NaCl solution for 30 min is composed of both metallic Cu and Cu(I), the latter being Cu_2O. The amounts of other oxidized copper species and oxygen forms are relatively small.

As is evident from Table 1, exposure of Cu–Bi alloy specimens to chloride solution resulted in a decrease of Bi content (in at.%) in the surface layer, except when a specimen with *ca*. 0.7 at.% Bi was placed into a corrosive medium for 30 min. Consequently, it may be inferred that the so-called dealloying of Cu–Bi alloy tends to occur during a contact of alloys with the chloride solution.

Figure 10 shows a typical Bi $4f_{7/2}$ spectrum from the Cu–Bi alloy (*ca*. 0.4 at.% Bi) specimen after exposure in 5% NaCl solution for 30 min. A comparison of E_b of two observed peaks, 158.8 and 159.4 eV, with the reference values of E_b indicates that these peaks can be attributed to Bi_2O_3 and BiOCl, respectively. Bi_2O_3 appears to be the main

Bi compound formed on the surface of the specimen.

Analysis of the XPS data (Table 1) also showed that the amount of chlorine was only slightly affected by t_{imm} when a Cu–Bi alloy specimen with the lowest content of Bi was used for the corrosion experiments. For the other Cu–Bi specimens, the change of chlorine content in the surface film with immersion time was quite similar, *viz*. it was almost halved with extending t_{imm}. The Cl/Na ratio (Table 1) was much higher than the value characteristic of NaCl, indicating the Cl bonding to the oxygenated species of metals. It was also found that, for the same duration of the corrosion experiments, the amount of chlorine somewhat increased with the initial amount of Bi in the alloy at t_{imm} = 30 min (Fig. 11), while there was no effect of the initial composition of alloy when t_{imm} was extended to 60 min.

After surface sputtering and removal of approximately 2 or 10 nm thick layers from the top surface, the contents of separate elements (in at.%) were found to change with depth as follows. In all instances, the Cu content and the ratio Cu/O increased in the inner parts of the surface layer, while the Bi content and the ratio Cu/Bi varied rather indefinitely (Table 1).

Interestingly, under conditions of our experiments oxygen could be detected even at a depth of *ca*. 10 nm. In this connection, it should be noted that while small amounts of oxygen were detected at a depth of *ca*. 2 nm when the untreated Cu–Bi alloy specimens were used for XPS examination (Table 1), no oxygen was detected at a depth of *ca*. 12 nm, as shown by separate experiments (not presented here). Therefore, the thickness of the corrosion product film formed during immersion for 60 min may be assumed to be no less than 10 nm. Such an assumption can be supported by the fact that small amounts of chlorine were still detected at this depth in XPS experiments (Table 1).

3.5. Interpretation of the corrosion behaviour of Cu–Bi alloys in a chloride medium

It will be recalled that although Bi was proposed to use in increasing Cu resistance to corrosion [30], there is still a lack of reliable data concerning this problem. As noted above, the experimental data were found to be not always unambiguously explainable. To our mind, one of the possible reasons is that the system Cu–Bi alloy – NaCl – dissolved O_2 is rather complicated. So, it might be difficult to propose any detailed description of Cu–Bi alloy corrosion process in a chloride solution under these circumstances. From the foregoing remarks, it should be of interest to reveal the main features of corrosion behaviour of alloys studied and to suggest their reasonable interpretation.

In order to define whether the aforementioned Marcus considerations on the influence of alloying elements [28] can be adoptable to the case of our interest, the respective data for the metal–metal bond strength ($\varepsilon_{M\text{-}M}$) and the metal–oxygen bond strength ($\varepsilon_{M\text{-}O}$) were correlated (Table 2). Examining this Table it becomes evident that both the $\varepsilon_{M\text{-}M}$ and the $\varepsilon_{M\text{-}O}$ for Bi are higher by about 20% than for Cu. It is also clear that the oxygenated compound of Bi is more stable than that of Cu. So, it seems reasonable to conclude that although Bi does not behave as a typical passivity promoter with respect to Cu, the data in Table 2 allow, in our mind, to assign this element to rather weak passivity promoters (*e.g*., in this regard, the pair Cu–Bi is relatively close to the pair Cu–Ni [28]). Then, passivation enhancement in the case of Cu–Bi alloys will be obtained due to formation of 3D bismuth(III) oxide involved into the composition of a passivating film.

It should be noted that the values of $\varepsilon_{M\text{-}M}$ and $\varepsilon_{M\text{-}O}$ or ΔH_{ads}(ox) are by no means the only ones that can determine the corrosion resistance of metals or alloys. For example, among the factors which can be expected to influence the degree of passivity of metals, the susceptibility to an attack by aggressive ions of both the underlying M surface and a passivating oxide was mentioned [54]. Generally, a departure from passivation may be indicated by the corrosion current, which may be taken to be composed of two components, as considered by Vijh [54]:

$$I_{cor} = I_M + I_{oxide}. \qquad (16)$$

It is obvious that the resistance of bare M to this attack is determined predominantly by $\varepsilon_{M\text{-}M}$. As regards the corrosive decomposition of a passivating oxide, the heat of the formation of oxide per equivalent, $-\Delta H_{equiv.}$, was proposed by Vijh [54] to be a proper representative parameter. Then, the correlation of $\varepsilon_{M\text{-}M}$ (Table 2) and $-\Delta H_{equiv.}$ (the latter quantities were derived from a relation $-\Delta H_{equiv.} = 0.5E_g$ [54], where the band gap energies E_g were taken as 1.8 and 2.7 eV for Cu_2O and Bi_2O_3 [55], respectively) for the studied metals gives the following pairs of these parameters: (i) 13.5 kcal and 20.8 kcal for Cu, and (ii) 16.5 kcal and 31.3 kcal for Bi, *i.e*. the latter metal has a stronger passivation tendency in a chloride medium. An extreme case of Cu, for which both the $\varepsilon_{M\text{-}M}$ and $-\Delta H_{equiv.}$ are low, was already presented by Vijh [54] as an example of the least passive metal among the 18 metals considered. As regards these properties of Bi, it can be easily shown

Table 2. **Selected data for the metal–metal ($\varepsilon_{M\text{-}M}$) and the metal–oxygen bond strength ($\varepsilon_{M\text{-}O}$) and for other thermodynamic properties of copper and bismuth**

Properties	Element			
	Cu		Bi	
Structure	fcc		rh	
Coordination number, Z	12		6[a]	
Heat of sublimation, ΔH_{subl}, kJ mol^{-1}	338.3		207	
$\varepsilon^{b}_{M\text{-}M}$, kJ mol^{-1}	56.4		69	
Initial[c] heat of adsorption of oxygen, ΔH_{ads}(ox), kJ mol^{-1}	293		461	
$\varepsilon^{d}_{M\text{-}O}$, kJ mol^{-1}	395	ca. 480		
Standard enthalpies of formation of crystalline compounds, $\Delta H^{o}_{f,298}$, kJ mol^{-1}	CuO:	–156 [56]	Bi_2O_3:	–575[56]
		–157.3 [57]		–307.6 [58]
		–159.8 [58]		
	Cu_2O:	–171 [56]		
		–168.6 [57]		
		–168.2 [54]		
Covalent bond dissociation energies of diatomic species, kJ mol^{-1}	CuO:	267 [56]	BiO:	339 [30,59]

Notes: [a] In view of the fact that Bi atoms are linked into sheets which are fitted together so that each atom has six neighbours – three on one side at a distance r_1 and three on the other side at a distance r_2, the ratio r_1/r_2 being equal to 1.149 [30], the coordination number for Bi, Z, was taken here as 6.

[b] $\varepsilon_{M\text{-}M}$ were calculated from the heat of sublimation of metal at 25 ° using an approximate relation: $\varepsilon_{M\text{-}M} = \Delta H_{subl}/(Z/2)$ [28].

[c] As proposed in [28], the initial heats of oxygen adsorption, *i.e.* adsorption at $\theta_{ox} \rightarrow 0$, were used. The numerical values of this parameter are taken from the literature sources, namely, for Cu directly from [28], and for Bi, as proposed in [58], after conversion from the value of standard enthalpy of the formation of Bi_2O_3, which was reported to be equal to –73.5 kcal mol^{-1} [58].

[d] $\varepsilon_{M\text{-}O}$ is related to the heat of oxygen adsorption by the relation: $\varepsilon_{M\text{-}O} = 0.5[\Delta H_{ads}(ox) + D(O_2)]$ [28], where $D(O_2)$ is the dissociation energy of O_2 taken here as 498 kJ mol^{-1} [59].

that Bi also belongs to the so-called less passivating metals (class B), because it lies below the separating line on a $\varepsilon_{M\text{-}M}$ *vs.* $-\Delta H_{equiv.}$ plot [54, 60]. One can recognize that a very similar situation was obtained for such alloying elements as Ni, Co and Fe [54, 60]. It should be emphasized that the foregoing considerations need to be experimentally confirmed.

The main results of the examination of Cu–Bi alloy specimens carried out in naturally aerated neutral 5% NaCl solution may be summarized as follows:

(*i*) the open-circuit potentials of Cu–Bi alloys were almost the same as for pure Cu;

(*ii*) the shape of the initial branches of cyclic voltammetric curves attributed to the oxygen reduction process depended on the nature of the electrode and on the length of immersion of electrodes in the chloride solution, indicating suppression of this process on Cu–Bi alloy, especially with a higher content of Bi and after a longer t_{imm};

(*iii*) the subsequent anodic behaviour of Cu–Bi alloys observed after a deep cathodic treatment was practically independent of t_{imm}, whereas that of pure Cu was strongly dependent on t_{imm};

(*iv*) without the preceding cathodic treatment, the anodic behaviour of pure Cu and Cu–Bi alloys was rather close, in particular in both cases the second anodic current peak disappeared;

(*v*) for both Cu and Cu–Bi alloy specimens, there was a general trend towards increasing R_p with t_{imm}, besides, R_p for Cu–Bi alloy with a lower content of Bi was somewhat larger as compared with pure Cu and another Cu–Bi alloy;

(*vi*) the instantaneous corrosion current for Cu and Cu–Bi alloys followed the time law with the parameters indicating that, firstly, dissolution of metal was controlled by diffusion through the corrosion product film and, secondly, I_{cor} for Cu–Bi (*ca.* 0.7 at.% Bi) as a function of t_{imm} decreased somewhat faster than that for pure Cu and Cu–Bi alloy (0.4 at.%); that likely implied the formation of a more protective corrosion product film on the former specimen;

(*vii*) the data of surface analysis showed that in the very top layer of specimen treated in chloride solution: (a) the presence of both Cu(0) and Cu(I) in the form of Cu_2O was highly expectable, whereas only very small amounts of cupric species might be

possible, (b) the presence of more than one type of oxygen was possible (O in the oxide lattice and in another oxygen-containing species), (c) the so-called dealloying of Cu–Bi alloys tended to occur during a contact of alloys with the chloride solution, (d) Bi_2O_3 appeared to be the main Bi compound formed on the surface of the specimen, (e) the Cl bonding to the oxygenated species of metals was possible;

(*viii*) the contents of separate elements changed with depth: (a) the copper content and the ratio Cu/O increased in the inner part of the surface layer, while the bismuth content and the ratio Cu/Bi varied rather indefinitely;

(*ix*) the thickness of the corrosion product film formed during immersion for 60 min was assumed to be no less than 10 nm;

(*x*) in the terms of the Marcus concept, Bi in the pair Cu–Bi can be assigned to rather weak passivity promoters.

Concerning the possibility of dealloying Cu–Bi alloys in chloride solutions, it should be mentioned that two basic mechanisms of binary alloys have been proposed in the literature (see, *e.g.* [61–63]): (*i*) simultaneous dissolution of both components of alloy followed by redeposition of one component (usually the more noble one), (*ii*) selective dissolution of one element from the alloy. The eventual dealloying of Cu–Bi alloys in chloride solutions may be presumed to occur likely according to the first model. Such a presumption can be supported by the Cu-enrichment of the surface layer of Cu–Bi alloy exposed to a corrosion medium and the high likelihood of the presence of elemental Cu along with Cu_2O in the very top layer. Obviously, in order to confirm more strictly this presumption, additional research is needed. In particular, it will be of importance to distinguish the corrosion behaviour of Cu–Bi alloys at short- and long- term exposures in chloride solution.

4. CONCLUSIONS

Corrosion currents for Cu–Bi alloys in aerated neutral 5% NaCl solution derived from the anodic Tafel slope and the polarization resistance were found to be a certain function of Bi content in the alloy specimen. Comparison of the data for Cu–Bi alloy with that for pure Cu was made. Surface analysis showed that the surface layer of a corroding Cu–Bi alloy specimen was mainly composed of Cu_2O, Bi_2O_3 and, with a high degree of probability, of elemental Cu formed most likely by redeposition during the dealloying.

In terms of the Marcus concept on the effect of alloying elements on the passivation of alloys [28], Bi in the pair Cu–Bi was assumed to be attributed to rather weak passivity promoters. Its effect on passivation enhancement may be due to formation of 3D Bi_2O_3 involved in the composition of a passivating film that was formed onto the surface of Cu–Bi alloy corroding in aerated chloride solution.

Received
16 November 2000
Accepted
27 November 2000

References

1. M. Pourbaix, *Lectures on Electrochemical Corrosion,* Plenum Press, New York–London (1973).
2. H. Kaesche, *Die Korrosion der Metalle*, Springer Verlag, Berlin–Heidelberg–New York (1979)
3. W. H. Smyrl, in *Comprehensive Treatise of Electrochemistry,* Vol. 4 (Eds. J. O'M. Bockris, B. E. Conway, E. Yeager and R. E. White), p. 97, Plenum Press, New York–London (1981).
4. *Corrosion Mechanisms in Theory and Practice,* (Eds. P. Marcus and J. Oudar), Marcel Dekker, Inc., New York–Basel–Hong Kong (1995).
5. A. I. Molodov, *Elektrokhimiya*, **17**, 534 (1981).
6. C. Deslouis, B. Tribollet, G. Mengoli and M.M. Musiani, *J. Appl. Electrochem.,* **18**, 374 (1988).
7. C. Deslouis, B. Tribollet, G. Mengoli and M. M. Musiani, *J. Appl. Electrochem.,* **18**, 384 (1988).
8. J. A. Ali, *Corros. Sci.,* **36**, 773 (1994).
9. F. Mansfeld, G. Liu, H. Xiao, C. H. Tsai and B. J. Little, *Corros. Sci.,* **36**, 2063 (1994).
10. W. A. Badawy, S. S. El-Egamy and A. S. El-Azab, *Corros. Sci.,* **37**, 1969 (1995).
11. M. Forslund and C. Leygraf, *J. Electrochem. Soc.,* **143**, 839 (1996).
12. E. D'Elia, O. E. Barcia, O. R. Mattos, N. Pébère and B. Tribollet, *J. Electrochem. Soc.,* **143**, 961 (1996).
13. O. E. Barcia, O. R. Mattos, N. Pébère and B. Tribollet, *Electrochim. Acta,* **41**, 1385 (1996).
14. Y. Feng, W.-K. Teo, K.-S. Siow, K.-L. Tan and A.-K. Hsieh, *Corros. Sci.,* **38**, 369 (1996).
15. Y. Feng, W.-K. Teo, K.-S. Siow and A.-K. Hsieh, *Corros. Sci.,* **38**, 387 (1996).
16. M. Itagaki, M. Tagaki, and K.Watanabe, *Corros. Sci.,* **38**, 1109 (1996).
17. K. E. Heusler, *Corros. Sci.,* **39**, 1177 (1997).
18. S. Sathiyanarayanan, M. Sahre and W. Kautek, *Corros. Sci.,* **41**, 1899 (1999).
19. M. Itagaki, T. Mori, and K. Watanabe, *Corros. Sci.,* **41**, 1955 (1999).
20. E. Cano, J. Simancas, J. L. Polo, C. L. Torres, J. M. Bastidas and J. Alcolea, *Materials and Corrosion,* **50**, 103 (1999).
21. W. H. Safranek, *The Properties of Electrodeposited Metals and Alloys. A Handbook,* Ch. 7, American Elsevier Publ. Comp., Inc., New York–London–Amsterdam (1974).
22. U. Bertocci and D. R. Turner, in *Encyclopedia of Electrochemistry of the Elements,* Vol. 2 (Ed. A. J. Bard), Ch. II-6, Marcel Dekker, Inc., New York (1974).

23. A. Brenner, *Electrodeposition of Alloys. Principles and Practice,* Vol. 1, Part III, Academic Press, New York–London (1963).
24. *Structure and Corrosion of Metals and Alloys. Atlas. Handbook* (Ed. E. A. Ulyanin), Ch. 5, Metallurgiya, Moscow (1989) (in Russian).
25. B. G. Ateya, E. A. Ashour and S. M. Sayed, *J. Electrochem. Soc.,* **141**, 71 (1994).
26. L. Burzyńska, A. Maraszewska and Z. Zembura, *Corros. Sci.,* **38**, 337 (1996).
27. A. Barbucci, G. Farné, P. Matteazzi, R. Riccierri and G. Cerisola, *Corros. Sci.,* **41**, 463 (1999).
28. P. Marcus, *Corros. Sci.,* **36**, 2155 (1994).
29. A. G. Massey, in *Comprehensive Inorganic Chemistry,* (Eds. J. C. Bailar Jr., H. J. Emeléus, R. Nyholm, and A. F. Trotman-Dickenson), Vol. 2, Ch. 27, Pergamon Press, Oxford–New York–Toronto–Sydney–Braunschweig (1975).
30. J. D. Smith, in *Comprehensive Inorganic Chemistry,* (Eds. J. C. Bailar Jr., H. J. Emeléus, R. Nyholm and A. F. Trotman-Dickenson), Vol. 2, Ch. 21, Pergamon Press, Oxford–New York–Toronto–Sydney–Braunschweig (1975).
31. F. Mansfeld, *Corrosion,* **29**, 397 (1973).
32. F. Mansfeld, *Corrosion,* **27**, 436 (1971).
33. C. D. Wagner, W. M. Riggs, L. E. Davis, J. F. Moulder and G. E. Muilenberg, *Handbook of X-Ray Photoelectron Spectroscopy,* Perkin Elmer Corp., Eden Prairie, Minessota (1979).
34. D. Briggs and M. P. Seach, *Practical Surface Analysis by Auger and X-Ray Photoelectron Spectroscopy,* John Wiley & Sons, New York (1983).
35. G. P. Cicileo, B. M. Rosales, F. E. Varea and J. R. Vilche, *Corros. Sci.,* **41**, 1359 (1999).
36. M. R. G. de Chialvo, R. C. Salvarezza, D. Vaquez Moll and A. J. Arvia, *Electrochim Acta*, **30**, 1501 (1985)
37. C. Kato and H. Pickering, *J. Electrochem. Soc.*, **131**, 1219 (1984).
38. T. Robert, M. Bartel and G. Offergeld, *Surface Sci.*, **33**, 123 (1972).
39. G. Schön, *Surface Sci.*, **35**, 96 (1973).
40. R. N. Lindsay and C. G. Kinniburgh, *Surface Sci.*, **63**, 162 (1977).
41. B. Millet, C. Fiaud, C. Hinnen and E. M. M. Sutter, *Corros. Sci.*, **37**, 1903 (1995).
42. R. M. Souto, V. Fox, M. M. Laz, M. Pérez and S. Gonsález, *J. Electroanal. Chem.*, **411**, 161 (1996).
43. L. Tommesani, G. Brunoro, A. Frignani, C. Monticelli, and M. Dal Colle, *Corros. Sci.*, **39**, 1221 (1997).
44. B. G. Baker, in *Modern Aspects of Electrochemistry*, No. 10 (Eds. J. O'M. Bockris and B. E. Conway), Ch. 2, Plenum Press, New York–London (1975).
45. R. W. Joyner, *Surface Sei.*, **63**, 291 (1977).
46. J. S. Hammond and N. Winograd, in C*omprehensive Treatise of Electrochemistry,* Vol. 8 (Eds. R. E. White, J. O'M. Bockris, B. E. Conway and E. Yeager), Ch. 8, Plenum Press, New York–London (1984).
47. V. V. Povetkin, Yu V. Rats and Yu. I. Ustinovshchikov, *Elektrokhimiya*, **30**, 26 (1994) (in Russian).
48. G. Deraubaix and P. Marcus, *Surf. Interface Anal.*, **18**, 39 (1992).
49. S. Haupt, U. Collisi, H. D. Speckmann and M. M. Strehblow, *J. Electroanal. Chem.*, **194**, 179 (1985).
50. E. Akiyama, A. Kawashima, K. Asami and K. Mashimoto, *Corros. Sci.*, **38**, 1127 (1996).
51. M. Johansson, J. Hedman, A. Bendtsson, M. Klasson, and R. Nillson, *J. Electron Spectr.*, **2**, 295 (1973).
52. R. J. Cole and P. Weightman, in *Metallic Alloys. Experimental and Theoretical Perspectives* (Eds. J. S. Faulkner and R. G. Jordan), NATO ASI Series. Series E: Applied Sciences, Vol. 256, p.27, Kluwer Academic Publishers, Dordrecht–Boston–London (1994).
53. R. K. Pandey, S. N. Sahu and S. Chandra, *Handbook of Semiconductor Electrodeposition*, Ch. 5, Marcel Dekker, Inc., New York–Basel–Hong Kong (1996).
54. A. K. Vijh, in *Modern Aspects of Electrochemistry*, No. 17 (Eds. J. O'M. Bockris, B. E. Conway and R. E. White), Ch. 1, Plenum Press, New York–London (1986).
55. J. W. Schultze and M. M. Lohrengel, *Electrochim. Acta*, **45**, 2499 (2000).
56. R. A. Lidin, L. L. Andreeva and V. A. Molochko, *Handbook of Inorganic Chemistry*, Khimiya, Moscow (1987) (in Russian).
57. G. M. Barrow, *Physical Chemistry*, 5th ed., McGraw-Hill Book Comp., New York–St. Louis–San Francisco etc. (1988).
58. K.-I. Tanaka and K. Tamaru, *J. Catalysis*, **2**, 366 (1963).
59. J. Emsley, *The Elements*, 2nd ed., p. 86, Clarendon Press, Oxford (1991).
60. N. D. Tomashov and G. P. Chernova, *Passivity and Protection of Metals Against Corrosion*, Plenum Press, New York (1967).
61. H. W. Pickering and C. Wagner, *J. Electrochem. Soc.,* **114**, 698 (1967).
62. H. W. Pickering and P. Byrne, *J. Electrochem. Soc.,* **116**, 1492 (1969).
63. P. S. Keir and M. J. Pryor, *J. Electrochem. Soc.,* **127**, 2138 (1980).

E. Ivaškevič, M. Gladkovas, A. Steponavičius, K. Leinartas, A. Sudavičius

VARIO IR VARIO-BISMUTO LYDINIO KOROZINĖS ELGSENOS NEUTRALIAME AERUOTAME CHLORIDO TIRPALE PALYGINAMASIS TYRIMAS

S a n t r a u k a

Cu ir Cu–Bi lydinių su įvairiais Bi kiekiais elektrocheminė elgsena aeruotame neutraliame 5% NaCl tirpale buvo tiriama katodinių ir anodinių potencialų intervaluose ir esant korozijos potencialui. Gauti eksperimentiniai įrodymai, kad katodinių potencialų intervale, kuriame vyksta deguonies redukcija, šis procesas ant Cu–Bi lydinių yra apsunkintas. Priklausomai nuo to, ar prieš potencialo skleidimą į teigiamesnių reikšmių pusę Cu ir Cu–Bi lydiniai buvo katodiškai poliarizuoti, ar nebuvo tokios poliarizacijos, šių bandinių anodinis tirpimas buvo skirtingas.

Korozinės srovės buvo skaičiuotos iš anodinio Tafelio nuolinkio ir poliarizacijos varžos. Nustatyta, kad korozinės srovės mažėja laikui bėgant ir kad jos yra tam tikra Bi kiekio lydinyje funkcija. RFES tyrimai parodė, kad koroduojančio bandinio paviršinis sluoksnis sudarytas daugiausia iš vario(I) oksido, bismuto(III) oksido ir, tikriau-

siai, elementinio vario. Padaryta prielaida, kad chloridas yra prijungiamas prie metalų deguoninių junginių.

Remiantis Marcus'o teorija, Bi poroje Cu–Bi yra, matyt, gana silpnas pasyvumo promotorius. Bi įtaka didinant pasyvumą gali būti paaiškinama tuo, kad susidaro 3D oksidas Bi_2O_3, kuris įeina į pasyvuojančio sluoksnio ant koroduojančio lydinio paviršiaus sudėtį.

Э Ивашкевич, М. Гладковас, А. Степонавичюс, К. Лейнартас, А. Судавичюс

СРАВНИТЕЛЬНОЕ ИССЛЕДОВАНИЕ КОРРОЗИОННОГО ПОВЕДЕНИЯ МЕДИ И СПЛАВА МЕДЬ-ВИСМУТ В НЕЙТРАЛЬНОМ АЭРИРОВАННОМ ХЛОРИДНОМ РАСТВОРЕ

Р е з ю м е

Электрохимическое поведение Cu и Cu–Bi сплавов с разным содержанием Bi в нейтральном 5% NaCl растворе исследовали в интервалах катодных и анодных потенциалов и при коррозионном потенциале. Получены экспериментальные доказательства, что в интервале катодных потенциалов, в котором происходит восстановление кислорода, этот процесс затруднен на Cu–Bi сплаве. В зависимости от того, подвергались или не подвергались катодной поляризации образцы Cu и Cu–Bi сплава перед последующей анодной разверткой потенциала, анодное растворение этих образцов является неодинаковым.

Коррозионные токи рассчитывали используя величины анодных тафелевских наклонов и поляризационных сопротивлений. Установлено, что коррозионные токи уменьшаются со временем и являются некоторой функцией от содержания Bi в сплаве. РФЭС исследования показали, что поверхностный слой корродирующего образца содержит, в основном, оксид меди(I), оксид висмута(III) и, с высокой степенью вероятности, элементную медь.

Высказано предположение, что в рамках концепции Маркуса висмут в паре Cu–Bi, по-видимому, является довольно слабым промотором пассивности. Воздействие Bi на усиление пассивности может быть объяснено тем, что формируется 3D оксид Bi_2O_3, который входит в состав пассивирующего слоя на поверхности корродирующего сплава.